sustainability

MDPI

Article

Predicting Changes in Population Exposure to Precipitation Extremes over Beijing–Tianjin–Hebei Urban Agglomeration with Regional Climate Model RegCM4 on a Convection-Permitting Scale

Peihua Qin [1,*], Zhenghui Xie [1], Binghao Jia [1], Rui Han [2] and Buchun Liu [2]

[1] State Key Laboratory of Numerical Modeling for Atmospheric Sciences and Geophysical Fluid Dynamics (LASG), Institute of Atmospheric Physics, Chinese Academy of Sciences, Beijing 100029, China
[2] Institute of Environment and Sustainable Development in Agriculture, Chinese Academy of Agricultural Sciences (CAAS), Beijing 100081, China
* Correspondence: qinpeihua@mail.iap.ac.cn

Abstract: In this study, we have investigated changes in precipitation extremes and the population's exposure to these extremes during 2091–2099 in China's Beijing–Tianjin–Hebei (JJJ) region relative to the historical period of 1991–1999. First, the regional climate model RegCM4, with a hydrostatic dynamic core, was run for east Asia, including China, at a 12 km resolution for 1990–1999 and 2090–2099. This model is forced by global climate model (GCM) MPI-ESM1.2-HR under the middle shared socioeconomic pathways (SSP245). The first year was used as a model spinup. Then, the 12 km results were used to force RegCM4 with a non-hydrostatic dynamic core (RegcM4-NH) at a 3 km convection-permitting scale over the JJJ region during the historical and future periods. Future precipitation extremes were predicted to increase over the whole of China and its four subregions, while decreases were predicted over the JJJ region. This may partly be caused by lower increases in specific humidity over the JJJ region. The percentage contributions of the three components of total population exposure, i.e., changes in exposure due to changes in the population, precipitation extremes and the joint impact of the population and extremes, were then analyzed. Changes in the population and wet extremes were closely related to changes in the total exposure over the JJJ region. The population is the dominant factor that most impacts the total exposure to dry extremes. Finally, changes in future population exposure to precipitation extremes per degree of warming were quantified for the JJJ region.

Keywords: CMIP6; convection-permitting; precipitation extremes; population exposure; RegCM4

check for updates

Citation: Qin, P.; Xie, Z.; Jia, B.; Han, R.; Liu, B. Predicting Changes in Population Exposure to Precipitation Extremes over Beijing–Tianjin–Hebei Urban Agglomeration with Regional Climate Model RegCM4 on a Convection-Permitting Scale. *Sustainability* **2023**, *15*, 11923. https://doi.org/10.3390/su151511923

Academic Editor: Subhasis Giri

Received: 29 June 2023
Revised: 25 July 2023
Accepted: 27 July 2023
Published: 3 August 2023

1. Introduction

Warmer climates increase the ability of the atmosphere to hold more water vapor, at a rate of around 6–7% per degree of warming, following the Clausius–Clapeyron (C-C) relationship [1,2]. This is expected to increase the occurrence of precipitation as well as its extremes at a super-C-C or sub-C-C scaling rate [3–9]. Thus, precipitation extremes are expected to become more frequent and more intense under warmer climates and to have more potential impacts on society, economics and natural ecosystems [3,10–13].

Compared to temperature, precipitation, as well as precipitation extremes, is difficult to realistically simulate due to its many impact factors and high spatiotemporal heterogeneity [14]. The global climate models (GCMs) used in the fifth and sixth phase of the Coupled Model Intercomparison Project (CMIP5 and CMIP6, respectively) [15,16] have been widely used to study current and future changes in global precipitation extremes [9,11,17]. They have also been adapted on regional scales in Africa [18,19], Asia [14,20–23], Europe [24], North America [25] and South America [26,27].

It remains challenging to project future precipitation extremes on the regional scale with a high resolution [28–30]. GCMs generally have relatively coarse spatial resolutions of around 100–200 km, which is not adequate to characterize the spatial distributions of precipitation extremes and their occurrence rates [28,31,32]. Climate models with high spatial resolutions can better simulate precipitation extremes as well as physical processes related to precipitation extremes, such as large-scale atmospheric rivers [5,33–36] and tropical cyclones [37,38]. Regional climate models (RCMs) describe dynamic and physical processes in more detail due to their high resolutions and can better reproduce spatiotemporal patterns of precipitation extremes over Asia [4,8,12,39], Europe [13,40], North America and South America [41]. GCMs are generally used to generate initial and boundary conditions (high temporal resolution of three-dimensional atmospheric temperature, specific humidity, atmospheric pressure, horizontal wind, etc.) to force RCM runs with high spatial resolutions for historical and future periods on a regional scale [42–45]. The regional climate model RegCM4, from the Abdus Salam International Center for Theoretical Physics [46], is widely used in climate studies [4,47–53]. The spatial resolutions of the majority of RegCM4 simulations are between 25 km and 60 km because the spatial resolution of the hydrostatic dynamic core is restricted to 10 km [54], physical processes are difficult to model and the GCMs used to generate initial and boundary conditions have relatively coarse spatial resolutions.

With increased computational ability, the spatial resolutions of RCMs have improved on the kilometer scale, i.e., the convection-permitting (CP) scale. This allows the characterization of spatial heterogeneities in more detail and explicit simulation of deep convection rather than the use of convection parameterization [55–58]. RCMs on the CP scale present obvious improvements in climate modeling [59–63] and generate more realistic precipitation extremes on the regional scale, including intensities, frequencies and spatiotemporal variabilities [28,64,65]. Lucas-Picher et al. [66] gave an overview of the latest developments and future directions of convection-permitting modeling with RCMs. Recently, a new version of RegCM-4.7, incorporating a non-hydrostatic dynamic core (RegCM4-NH) at a CP resolution [54], was developed to improve climate simulations [54,67–69].

The Beijing–Tianjin–Hebei (hereafter known as JJJ, since "Ji" is the abbreviation of Hebei province; Figure 1) region, a typical urban agglomeration in China, has encountered fast urbanization and rapid population growth in the last decades. This may affect the climate, and populations are at an increased risk of facing more frequent and intense climate extremes [70–72]. Besides the intensity and frequency of climate extremes, their effects also depend on how many people are subjected to them [31,73–77]. Increased population exposure to extremes, which is generally defined using extreme indices multiplied by the amount of people subjected to the extremes, is likely to negatively impact human lives [31,74,78,79].

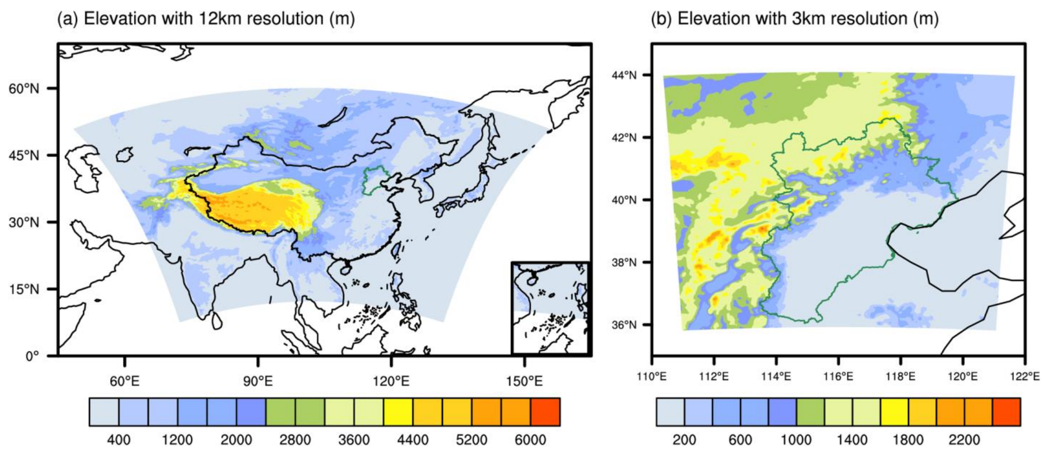

Figure 1. The RegCM4 model domains with grid sizes of 12 km (**a**) over the East Asia region and 3 km (**b**) over the Beijing–Tianjin–Hebei (JJJ) region, with elevation (m). The area inside the green polygon is the JJJ region.

In the present study, we have investigated changes in precipitation extremes and the population exposure to these extremes projected over the whole of China for 2091–2099 and in the JJJ region relative to the historical period of 1991–1999, i.e., the changes in extremes in one century. The rate of exposure to precipitation extremes per degree of warming was also quantified for the JJJ region. First, RegCM4 with a hydrostatic dynamic was run over East Asia at a 12 km resolution for the historical (1990–1999) and future periods (2090–2099) as usual [69], due to the expensive computing costs and large storage needed for regional climate modeling, especially on the CP scale. Initial and boundary conditions were generated with the Max Planck Institute Earth System Model (MPI-ESM1.2-HR), which uses an ECHAM6.3 atmospheric model coupled with an MPIOM1.62 ocean model in CMIP6 under the central shared socioeconomic pathways (SSP245) [80]. This model has been widely used because it results in more realistic climate modeling and is well-suited for prediction and mechanism studies [21,81]. Then, RegCM4-NH at a 3 km resolution was run for JJJ in the historical and future periods, forced by the former 12 km results from RegCM4 with the hydrostatic core. We have evaluated the performance of RegCM4 with the hydrostatic core in China and of RegCM4-NH over the JJJ region. Oleson et al. (2013) have shown that RegCM4-NH could simulate the spatial distribution of annual and summer precipitation in more detail over JJJ and that RegCM4-NH with the CLM4.5 land surface component [82] has shown the best performance in simulating precipitation extremes compared to other experimental setups. Here, we have investigated changes in future precipitation extremes predicted for 2091–2099 over four subregions of China (NW: Northwest China; NC: North China; SC: South China; and TP: Tibetan Plateau) and JJJ urban agglomeration, as well as their possible mechanisms, using RegCM4 with a hydrostatic core or RegCM4-NH (Figure 2). Finally, future changes in exposure to precipitation extremes, such as exposure change per degree of temperature increase, were investigated for JJJ, and the respective contributions of the changes in the extremes and the changes in the population to exposure changes were quantified.

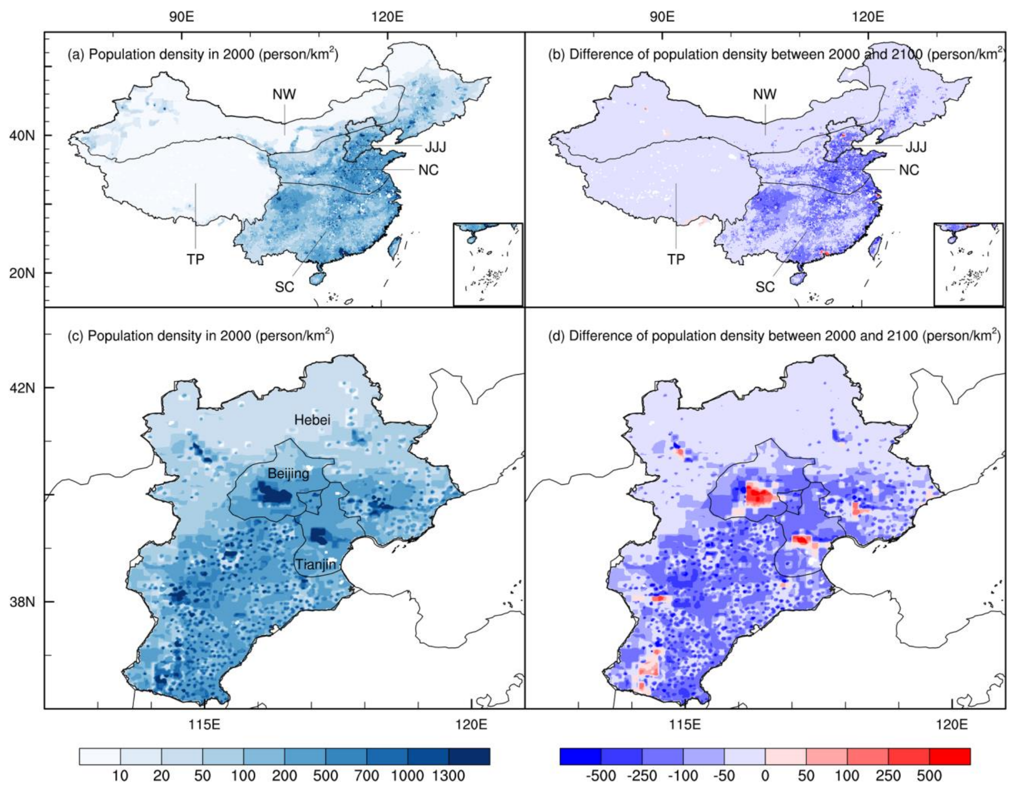

Figure 2. Spatial distributions of population density in 2000 at a 0.1° × 0.1° resolution in China (**a**) and in the Beijing–Tianjin–Hebei urban agglomeration (JJJ) at a 0.025° × 0.025° resolution (**c**) and their future changes in 2100 relative to 2000 (**b**,**d**).

2. Data and Model

2.1. Data

A spatial distribution of the global population at a resolution of 1 km from 2000 to 2100 under the middle SSP245 scenario, which was downscaled by Gao [83] from a population with a 1/8° spatial resolution [84] and has been widely used [31,73,85], was applied here. The population data were regridded to 0.1° × 0.1° (~10 km) in China and to 0.025° × 0.025° (~2.5 km) over JJJ, with distance weight. Because this dataset has begun in 2000 and provides data points for every 10 years, we used the spatial distributions of the population in 2000 and 2100 to represent the historical population during 1991–1999 and future population during 2091–2099, respectively.

The outputs of horizontal wind, the air temperature, specific humidity and the sea surface temperature with MPI-ESM1.2-HR during 1990–1999 and 2090–2099, under the SSP245 scenario, were used to generate the initial and boundary conditions (such as three-dimensional air temperature, water vapor, horizontal wind, two-dimensional surface temperature, etc.) for RegCM4, with hydrostatic and non-hydrostatic dynamic core runs. These outputs were at a temporal resolution of six hours and over 192 × 384 grid points, with a spatial resolution of about 0.9°. The daily precipitation from MPI-ESM1.2-HR was used to generate precipitation extremes to compare with those based on RegCM4.

2.2. Regional Climate Model Description and Experimental Design

The regional climate model RegCM4.7 from ICTP [46] was dynamically downscaled to East Asia, with the whole of China and the JJJ region included (Figure 1). RegCM4.7 can carry out simulations with a hydrostatic or a non-hydrostatic dynamic core [54]. In a similar experimental setup, RegCM4 with a hydrostatic dynamic core was used to dynamically downscale MPI-ESM1.2-HR under the SSP245 scenario in China, with a 12 km resolution of 600 × 450 grids for the historical period of 1990–1999 and the future period of 2090–2099 (RCM_CLM_12km). Due to expensive computing costs and the large storage required for the test and simulation results as well as the forcing data, only the middle SSP245 scenario, which is consistent with historical development rates [80], was adopted, as in a previous study [31], to force RegCM4 to study precipitation extremes. In future work, RegCM4 forced by different scenarios will be used to better investigate future precipitation extremes. The land surface component was adopted as the CLM4.5 scheme [82], which presented more spatial details of this surface. The Grell convection scheme [86] for land and ocean and the WSM5 microphysics scheme [87] were used as cumulus convection and explicit cloud microphysics simulations for RegCM4 with hydrostatic and non-hydrostatic cores, respectively, after careful sensitivity tests, since kilometer grid size is usually considered a gray-zone resolution and convection parametrization will still be needed [68]. The 12 km results of RegCM4 were then used to force RegCM4-NH in a one-nest way over the JJJ region at a 3 km resolution on a 300 × 300 grid (RCM_CLM_12km). The first year of each simulation was used as a model spinup, and only the last nine years were used for this analysis. RegCM4 with both hydrostatic and non-hydrostatic dynamics used the CLM4.5 land surface component, since RegCM4 with CLM4.5 performs better at simulating mean and extreme precipitation [82]. The outputs of RegCM_CLM_12km and RegCM_CLM_3km were regridded to 0.1° × 0.1° (~10 km) in China and 0.025° × 0.025° (~2.5 km) over JJJ, with distance weight, to study the population exposure to precipitation extremes. Additionally, this study has mainly investigated the impacts of current and future CMIP6 forcing on precipitation extremes without land use changes as limitations, and the contributions of global atmospheric circulation and regional land use are expected to be revealed in the near future.

2.3. Precipitation Extreme Indices

Different definitions of precipitation extremes may affect the conclusions of climate change studies [88]. In this study, we have used extreme precipitation indices defined by the Expert Team on Climate Change Detection and Indices (ETCCDI) [89]. These indices have been widely used in studies on climate extremes [90–94]. Four precipitation extreme indices from the ETCCDI were used to study changes in future extremes: the annual total precipitation on days when the daily precipitation would exceed 95% percentile of the daily precipitation (R95p, unit: mm); the annual maximum 5-day consecutive precipitation (Rx5day, unit: mm); the annual maximum consecutive days with precipitation values greater than 1 mm (CWD; unit: days), and that of those less than 1 mm (CDD; unit: days).

3. Results

3.1. Changes in the Future Population in China and the JJJ Region

Figure 2 shows the spatial distribution of the population density in China in 2000 at a spatial resolution of 0.1° × 0.1° and in the JJJ region at a 0.025° × 0.025° resolution, as well as their predicted changes in 2100 relative to 2000. The gradient of the spatial distribution of the population density in China followed the spanning dry, semi-dry, semi-humid and wet complex climate types from the northwest to the southeast of China (Figure 2a). The majority of people live in Northern and Southern China, which belongs to the East Asian monsoon region [95]. By 2100, the population density in China is predicted to moderately decrease, especially in Northern and Southern China under the SSP245 scenario (Figure 2b) [31]. Chen, Guo, Wang, Cai, Wang and Wang [95] estimated that the population in China will increase to a peak, ranging from 1.44 to 1.48 billion around 2027–2034 m and then decrease continuously until 2100.

As a typical urban agglomeration of China, the JJJ region has a high population density due to fast urbanization (Figure 2c). The population is mainly concentrated in the downtown areas of Beijing, Tianjin and the large cities of Hebei (dark regions in Figure 2c). Similarly to the changes in the future population density in China, the population density over the JJJ region was predicted to decrease by 2100 (Figure 2d). The only exception was a moderate increase in the population density of the high-density downtown areas of JJJ, which means that more and more people will move to those areas in the future.

3.2. Changes in Future Precipitation Extremes

In a previous study, we evaluated the performances of RegCM4 with the hydrostatic dynamic core in China and the non-hydrostatic dynamic core over the JJJ region in simulations of historical mean and extreme precipitation during 1991–1999 [82]. High-resolution RCMs can characterize the spatial distribution of precipitation extremes in high detail and exhibit good performance in simulating precipitation extremes.

Figures 3 and 4 show the spatial distributions of changes in the precipitation extreme indices in China, for the future period of 2091–2099, and the JJJ region, relative to the historical period of 1991–1999, using MPI-ESM1.2-HR, RCM_CLM_12km and RCM_CLM_3km. Here, the absolute changes in precipitation extremes were presented rather than the relative changes, since absolute changes in extremes directly contribute to changes in population exposure to extremes [48]. Reasonably simulating mean and extreme precipitation is a great challenge, as extremes in precipitation depend on many physical processes and have high spatiotemporal heterogeneity [14]. In spite of the fact that most areas of China are generally projected to have warmer climates by the end of the 21st century [4], heavy precipitation extremes R95p and Rx5day, simulated with both MPI-ESM1.2-HR and RCM_CLM_12km, have shown large spatial variations (Figure 3a–d). The future R95p extremes simulated with MPI-ESM1.2-HR and RCM_CLM_12km showed increases with rates of 3.54 and 13.62 mm, respectively, over the NW subregion; 15.14 and 28.08 mm, respectively, over the TP subregion; 26.77 and 31.45 mm, respectively, over the NC subregion; and 30.95 and 3.38 mm, respectively, over the SC subregion (Figures 3 and 5a). RegCM4_CLM4_12km showed more spatial details of precipitation extremes due to its higher resolution compared to the MPI-ESM1.2-HR results. The R95p in the whole of China was predicted to increase by 12.62 and 19.90 mm with MPI-ESM1.2-HR and RCM_CLM4_12km, respectively (Figure 5a). Future changes in the Rx5day and R95p showed similar results, with increases over China as well as its four subregions, with both MPI-ESM1.2-HR and RCM_CLM_12km (Figure 3b,d).

These increases in the R95p and Rx5day over the whole of China and its subregions are probably due to the warmer climate, which will increase the ability of the atmosphere to hold more water vapor following the C-C relationship [1,2] and the specific humidity in the atmosphere in general (Figure 6b).

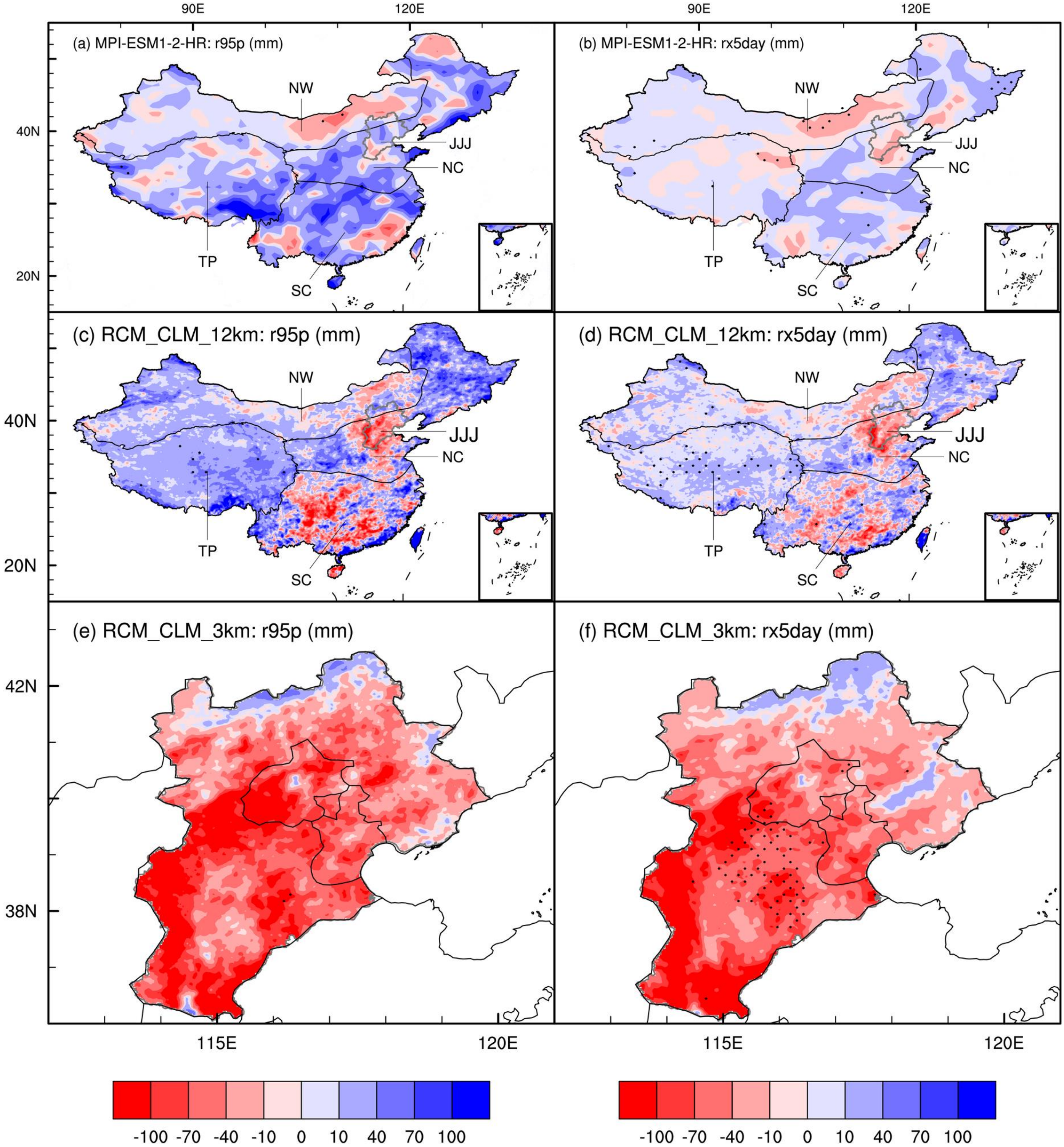

Figure 3. Spatial distributions of changes in precipitation extremes (R95p and Rx5day) during 2091−2099 in China and JJJ relative to the historical period of 1991−1999, with MPI−ESM1.2−HR, RCM_CLM_12km and RCM_CLM_3km. Stippling means changes are significant on the level of 0.05 with a t−test.

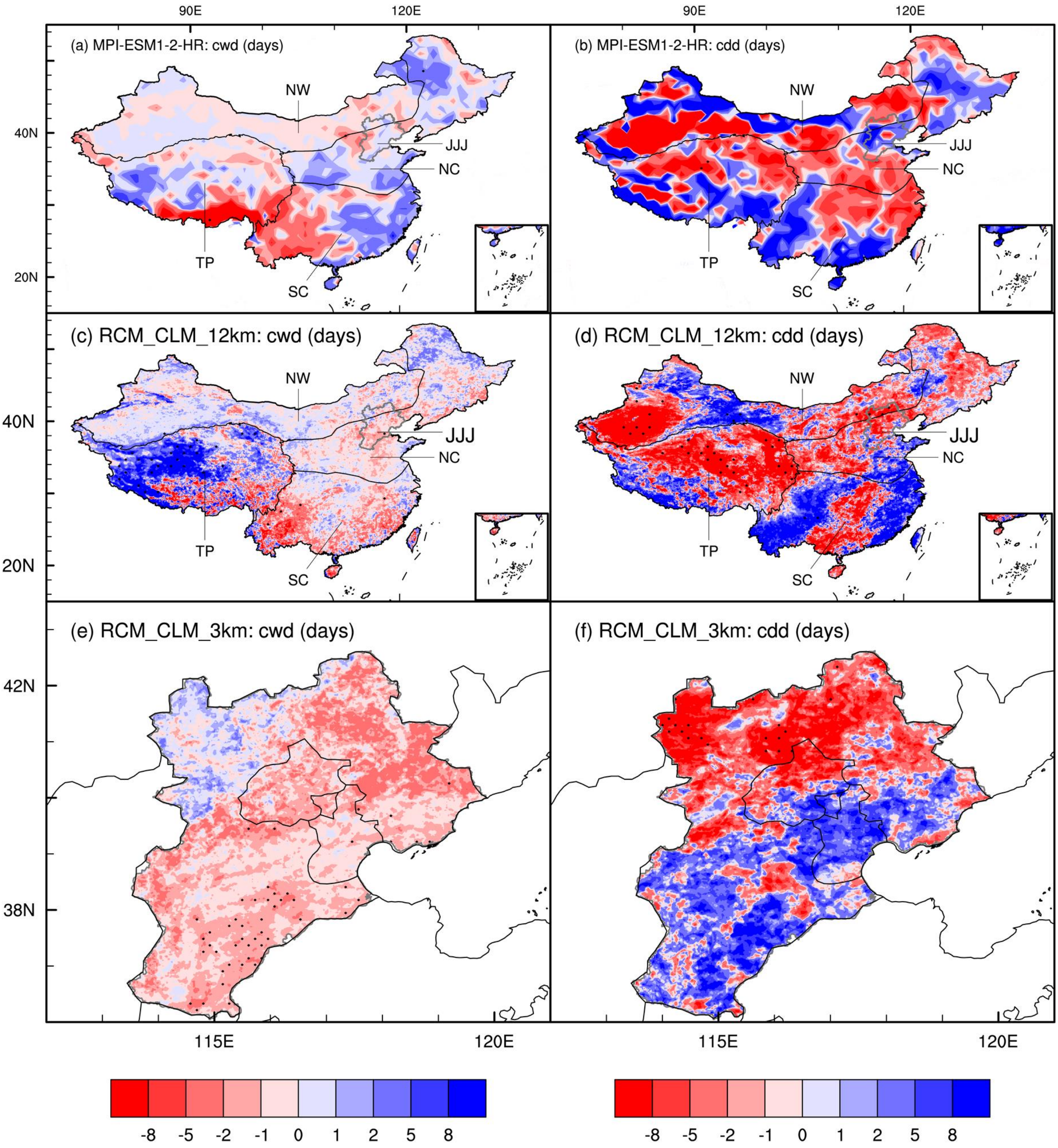

Figure 4. Same as Figure 3, but for extreme precipitation indices CWDs and CDDs.

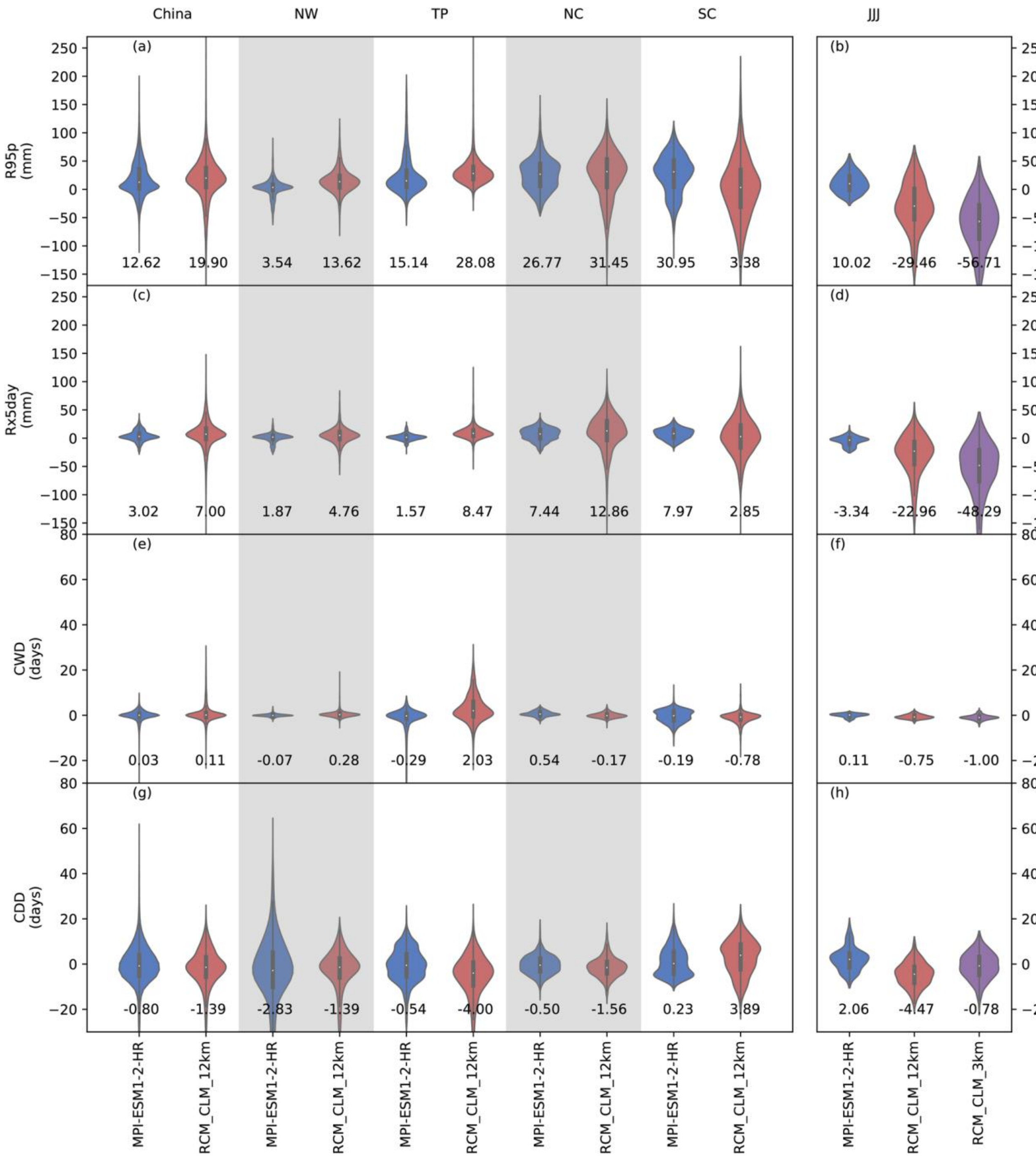

Figure 5. Violin plots of changes in four precipitation extremes during 2019–2099 relative to the historical period of 1991−1999 with MPI−ESM1.2−HR, RCM_CLM_12km and RCM_CLM_3km over China and its four subregions (**a**,**c**,**e**,**g**) and the JJJ region (**b**,**d**,**f**,**h**). The value beneath each violin plot is the median of the precipitation extremes over the whole of China and its four subregions as well as the JJJ region.

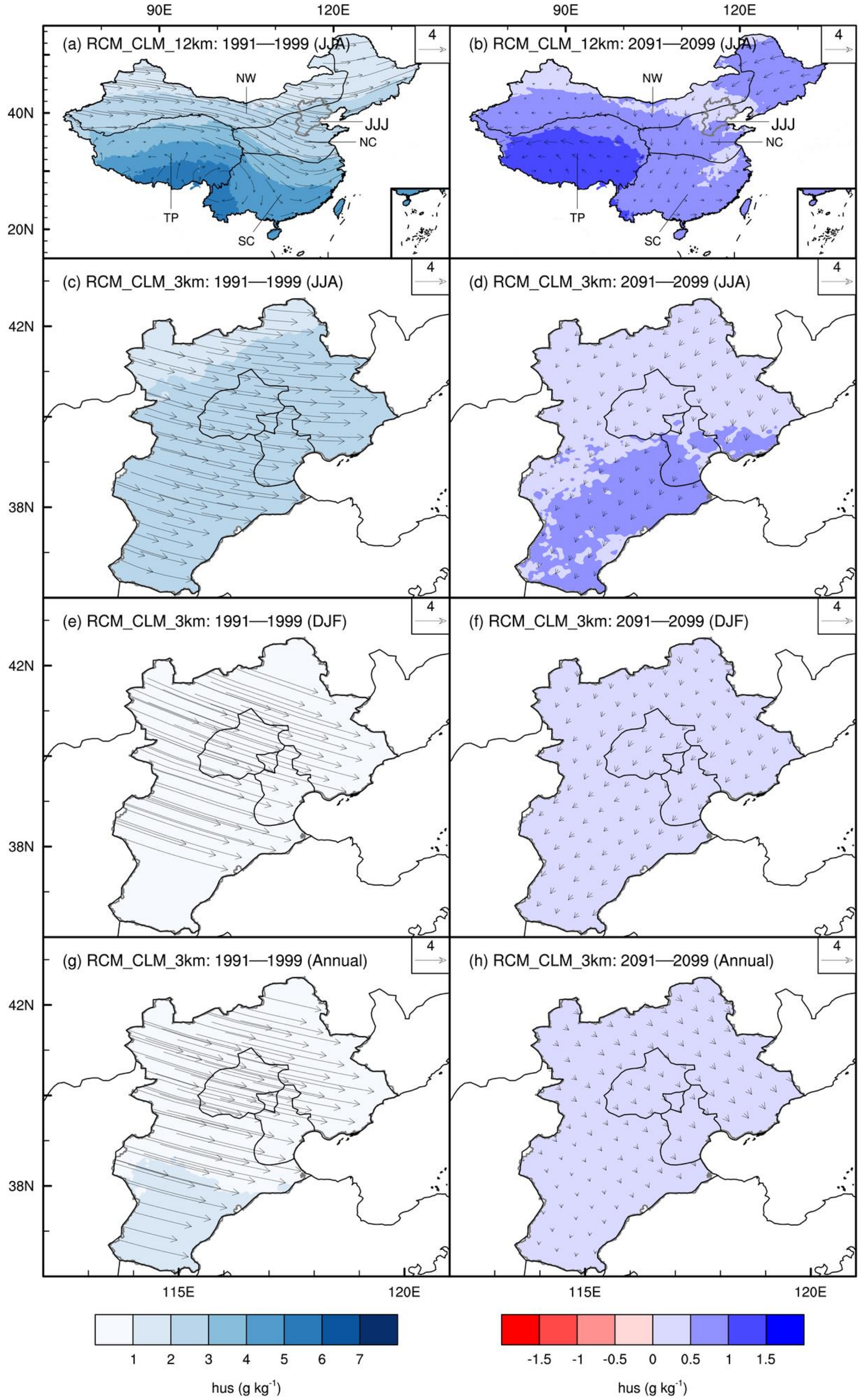

Figure 6. Spatial distributions of climatic summer (JJA) wind vectors and specific humidity at 500 hPa during 1991−1999 and their predicted future changes during 2091−2099 over China and the JJJ region with RCM_CLM_12km (**a**,**b**) and RCM_CLM_3km (**c**,**d**), respectively. The wind vectors and specific humidity values over the JJJ region are also shown for winter (**e**,**f**) and annually (**g**,**h**).

RegCM4-NH produced more elaborate spatial distributions of the R95p and Rx5day over the JJJ region (Figure 3e,f). Due to a high spatiotemporal variability of the mean and extreme precipitations, changes in the future R95p and Rx5day over a small region showed different results than those of the larger area. R95p and Rx5day with RCM_CLM_3km over JJJ were found to moderately decrease by 56.71 and 48.29 mm, respectively, in spite of low increases in specific humidity (Figure 5d), with a larger decrease than simulated with RCM_CLM_12km, which gave decrease rates of 29.49 and 22.96 mm, respectively. The probable reason for this is the lower increases in future specific humidity over the JJJ region compared to other areas in China (Figure 6b,d), with slight increases in specific humidity and no obvious changes in horizontal wind at 500 hPa over JJJ in the summer (JJA) or winter (DJF) or the annual mean (Figure 6c–h). Land surface conditions such as land use and topography might greatly impact changes in precipitation extremes due to the high spatial resolution of 3 km used. Here, the mechanisms of the changes in precipitation extremes have been given in brief, and more detailed mechanism analysis will be carried out in the future.

Compared to R95p and Rx5day, changes in future consecutive wet days (CWDs) were not obvious, with increasing or decreasing rates ranging from −0.78 to 2.03 days in China and its four subregions with MPI-ESM1.2-HR and RCM_CLM_12km, respectively (Figure 5e). Similar results for CWDs over JJJ with RCM_CLM_3km showed slight decreases in the future and similar spatial patterns from those shown for R95p and Rx5day (Figure 5f). As a dry precipitation extreme index, consecutive dry days (CDDs) generally present negative change rates compared to R95p and Rx5day (Figure 4b,d,f). The CDDs estimated with both MPI-ESM1.2-HR and RCM_CLM_12km were found to decrease at rates of 2.83 and 1.39 days, respectively, over the NW subregion; 0.54 and 4.00 days, respectively, over the TP subregion; and 0.50 and 1.56 days, respectively, over the NC subregion and increase at rates of 0.23 and 3.89 days, respectively, over the SC subregion. RCM_CLM_3km showed a lower CDD decrease rate, of 0.78 days, compared to RCM_CLM_12km, which produced a CDD decrease rate of 4.47 days. RCM_CLM_3km presented decreased and increased CDDs over the north and south of the JJJ region, respectively (Figure 4h), which might be due to the different terrain in the mountain and plain regions (Figure 1b). Mountain areas might present more complex climates relative to plain regions [96], and more detailed analysis together with that of different land use will be performed in specific studies.

Therefore, precipitation extremes with higher spatial resolution modeling may result in different conclusions than those predicted by coarse models. The inclusion of physical processes and higher-resolution input data should also be developed to improve high-resolution climate models.

3.3. Changes in Population Exposure to Precipitation Extremes

After investigation of the changes in the future population and precipitation extremes in China and the JJJ region, the changes in the future population's exposure to these precipitation extremes over the JJJ region were analyzed using RCM_CLM_3km. Population exposure to precipitation extremes is quantified using precipitation extreme indices multiplied by the amount of people exposed [31,74,78]. This is expressed as EXPO = POP × PE, where EXPO is the population exposure to precipitation extreme indices, POP is the population and PE represents extreme indices. Changes in population exposure are decomposed into three components: the impact of extreme precipitation, the impact of the population and the joint impact of the extremes and the population [79,97]. This is expressed as

$$\Delta \mathrm{EXPO} = \mathrm{POP} \times \Delta \mathrm{PE} + \Delta \mathrm{POP} \times \mathrm{PE} + \Delta \mathrm{POP} \times \Delta \mathrm{PE}, \quad (1)$$

where ΔEXPO represents changes in the population's exposure to extreme precipitation; POP and ΔPOP are the historical population and future changes in the population, respectively; and PE and ΔPE are the historical precipitation extreme index and future changes in precipitation extremes, respectively.

Figures 7–10 show the population exposure to R95p during the historical period of 1991 to 1999; projected future changes in 2091–2099, relative to the historical period; and the percentage contributions from changes in precipitation extremes, changes in the population and combined changes in precipitation extremes and population. The spatial patterns of the historical population's exposure to the R95p and Rx5day wet extreme indices in the JJJ region were generally dominated by the spatial distribution of the population density, i.e., more exposure to R95p and Rx5day over areas of JJJ with higher population densities (Figures 7a and 8a). This is consistent with global results [31]. Because of a moderate decrease in the future population over most of the JJJ area except in some downtown regions (Figure 2), as well as less R95p and Rx5day over most of the JJJ region (Figures 3 and 5b,d), changes in the future population's exposure to R95p and Rx5day are expected to decrease over almost all of JJJ, especially over the south, with decreases of more than 10×10^4 person mm (Figures 7b and 8b). Changes in exposure to both R95p and Rx5day due to changes in the population and the extreme indices will present negative contributions to the total changes in the population's exposure to these two indices over most of JJJ. These changes can range from about -60 to 20×10^4 person mm and from -40 to 10×10^4 person mm, except in some downtown regions with projected increasing populations for the future (Fgures 7d,e and 8d,e). The contributions of the changes in population exposure due to the combined impacts of the population and extreme indices were positive but had lower absolute values compared to the impacts due to changes in either the population or extreme indices alone, representing no more than 50,000 person mm over most of JJJ (Figures 7f and 8f). The percentage of absolute contribution from each component of the changes in the population exposure in Figures 7c, 8c, 9c and 10c is defined as

$$\mathrm{abs}(\mathrm{POP} \times \Delta \mathrm{PE})/(\mathrm{abs}(\mathrm{POP} \times \Delta \mathrm{PE}) + \mathrm{abs}(\Delta \mathrm{POP} \times \mathrm{PE}) + \mathrm{abs}(\Delta \mathrm{POP} \times \Delta \mathrm{PE})) \times 100\%, \quad (2)$$

with the spatial average population exposure over the JJJ region, where abs(•) is the absolute value operator. Predicted changes in the future R95p and population over JJJ represented the dominant contributions to the total exposure changes in R95p, with percentages of 43.47% and 44.30%, respectively, while the combined impact of R95p and the population represented 12.23% (Figure 7c). The percentages of the three components of exposure to Rx5day over the JJJ region were 47.92%, 38.37% and 13.70%, respectively.

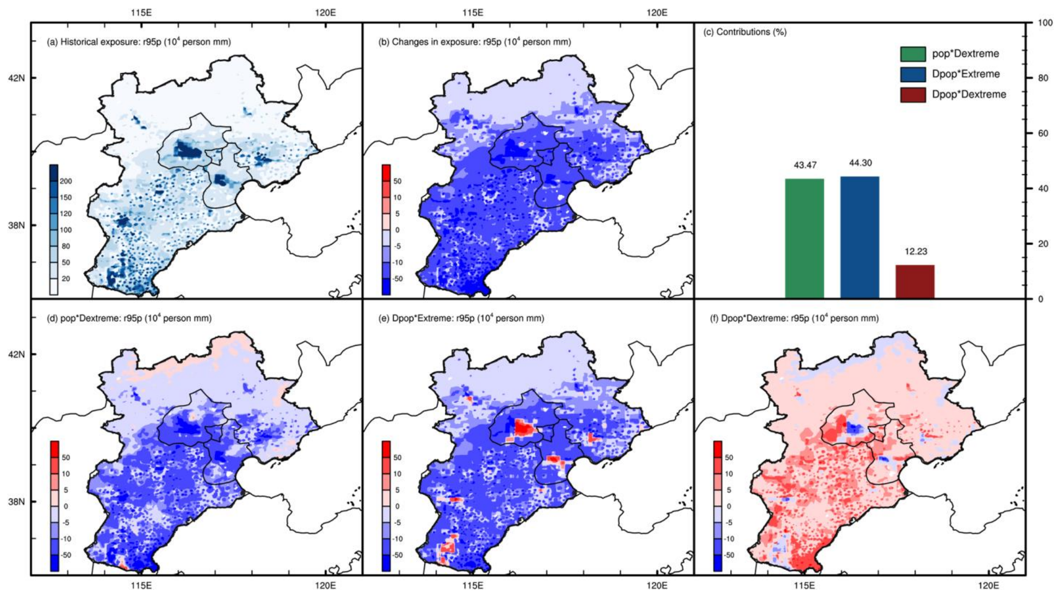

Figure 7. Historical (1991–1999) population exposure (unit: 10^4 person mm) to R95p (**a**) and predicted future changes in 2091–2099 (**b**), percentage contributions (**c**) due to changes in precipitation extremes (**d**), changes in the population (**e**) and combined changes in precipitation extremes and the population (**f**).

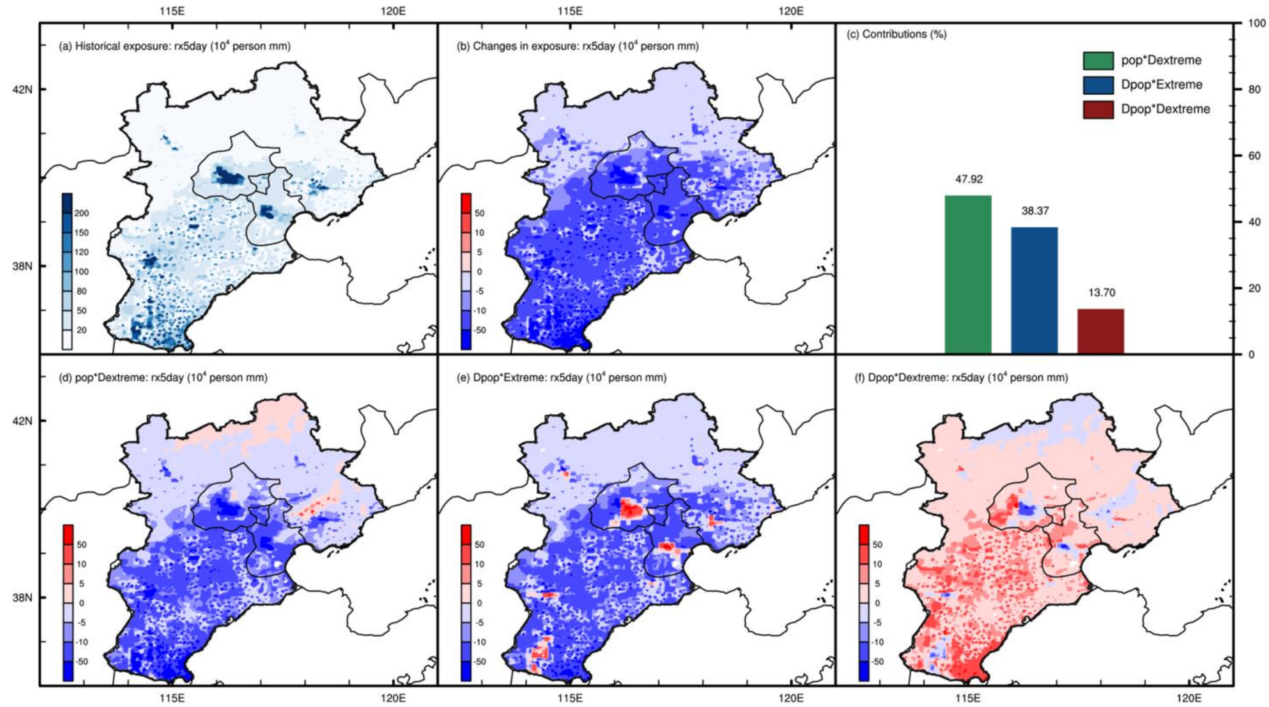

Figure 8. Same as Figure 7, but for Rx5day.

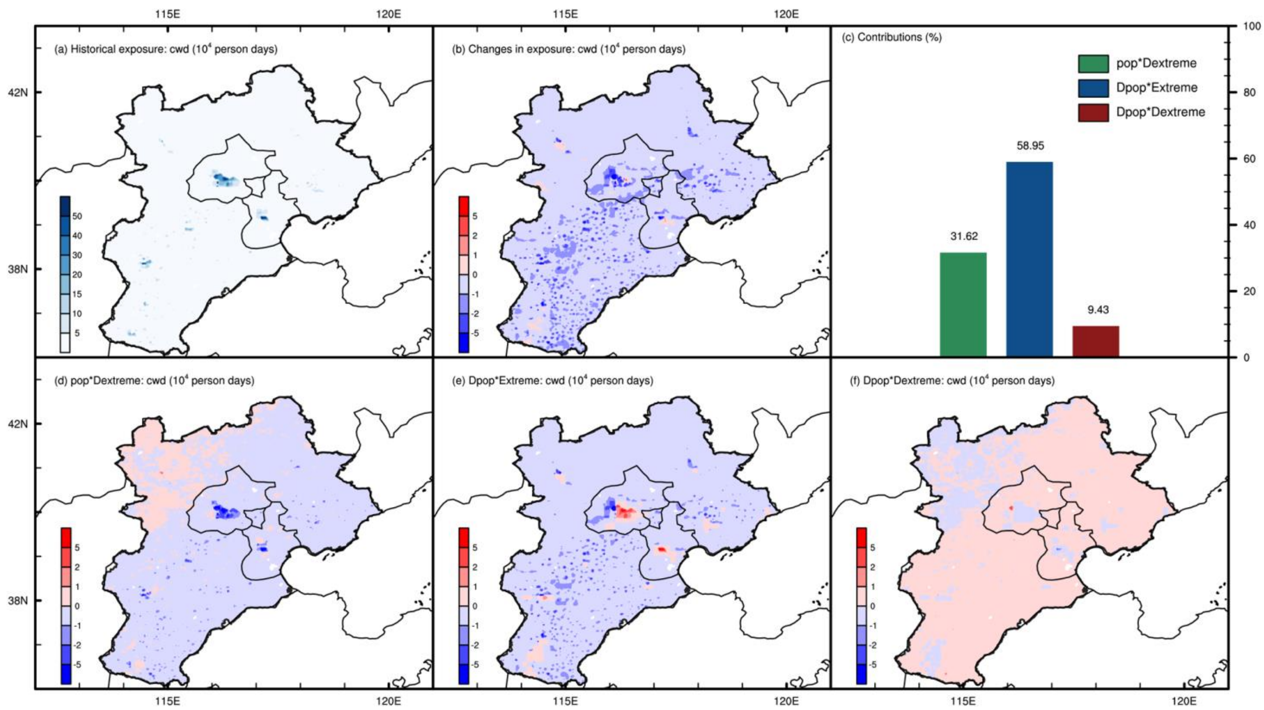

Figure 9. Same as Figure 7, but for CWDs (unit: 10^4 person days).

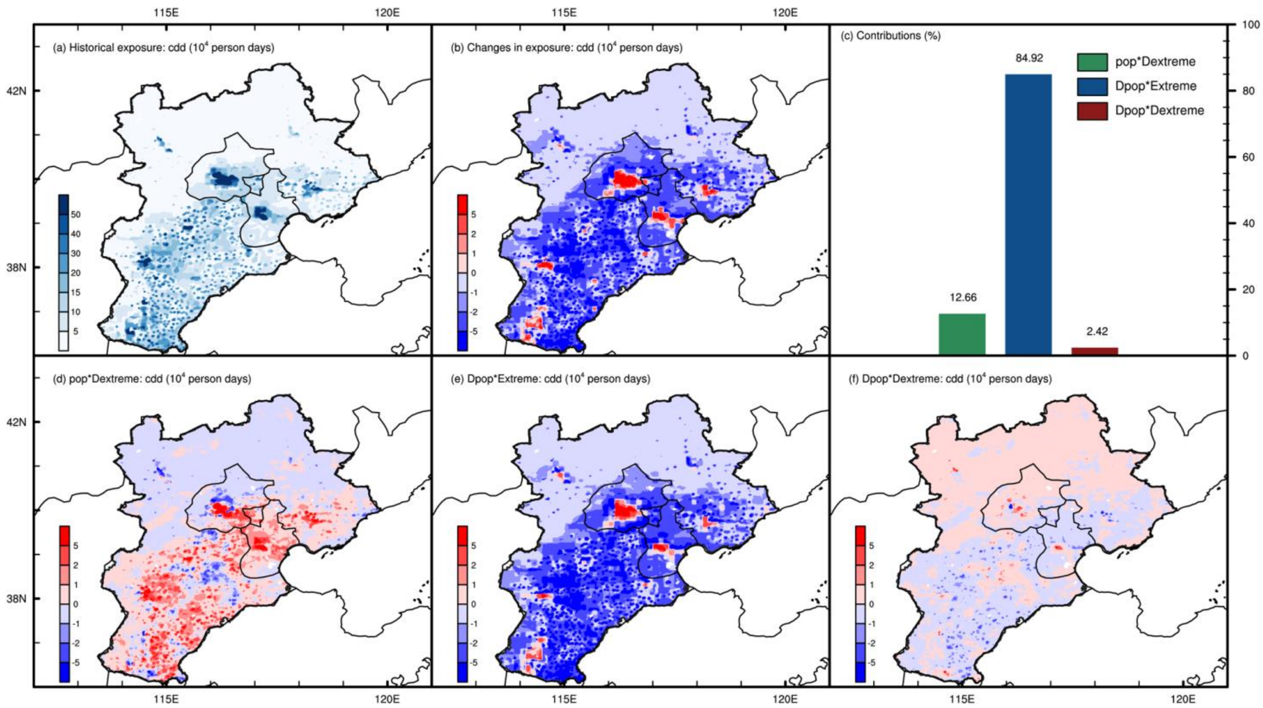

Figure 10. Same as Figure 7, but for CDDs.

Similarly to the simulated exposure changes to R95p and Rx5day, the total population exposure to CWD decreased over most of JJJ but with relatively small rates of no more than 1 $\times$ 10^4 person days, partly due to small changes in future CWDs (Figures 4e, 9 and 11c). We found negative contributions to changes in the total exposure due to changes in the future population and CWDs but positive contributions to the combined changes in the population and CWDs, with percentage contributions of 31.62%, 58.95% and 9.43%, respectively (Figure 9).

Unlike the total exposure to R95p, Rx5day and CWD wet precipitation extreme indices, the changes in the total population exposure to CDDs were projected to increase over the large downtown areas of JJJ but decrease over other parts of JJJ (Figure 10d). This is consistent with the spatial distribution of changes in the projected future population (Figure 2d). The total exposure to CDDs over the JJJ region ranged from about -5 to 5×10^4 person days (Figure 11d). The percentage contribution of the population changes to the total exposure was 84.92%: largely dominant among the three components of the total population (Figure 10c).

Finally, we quantified the changes in the total population exposure to precipitation extremes with air surface temperature (TAS) increases over the JJJ region, which have been widely adopted in previous studies [4]. Changes in the population exposure to precipitation extremes per degree of warming were calculated through spatial mean changes in the precipitation extremes and the surface air temperature over the JJJ region, with a sample size of 36,098. The multi-year annual mean temperatures in 1991–1999 and 2091–2099, which were calculated with the daily temperature mean in each grid of the JJJ region, represent the climatological temperatures during the historical and future periods, respectively. The increase rate of the TAS over JJJ generally ranged from about 2.7 to 3.5° (Figure 11). Under warmer climates in the period of 2091–2099, the expected changes in the total population exposures to R95p, Rx5day, CWDs and CDDs showed decreases of 7.37×10^4 person mm, 5.84×10^4 person mm, 0.15×10^4 person days and 0.64×10^4 person days, respectively, and these changes are significant at the 0.05 level using a *t*-test with grid-point numbers of 12,925, 25,251, 32,178 and 27,451, respectively.

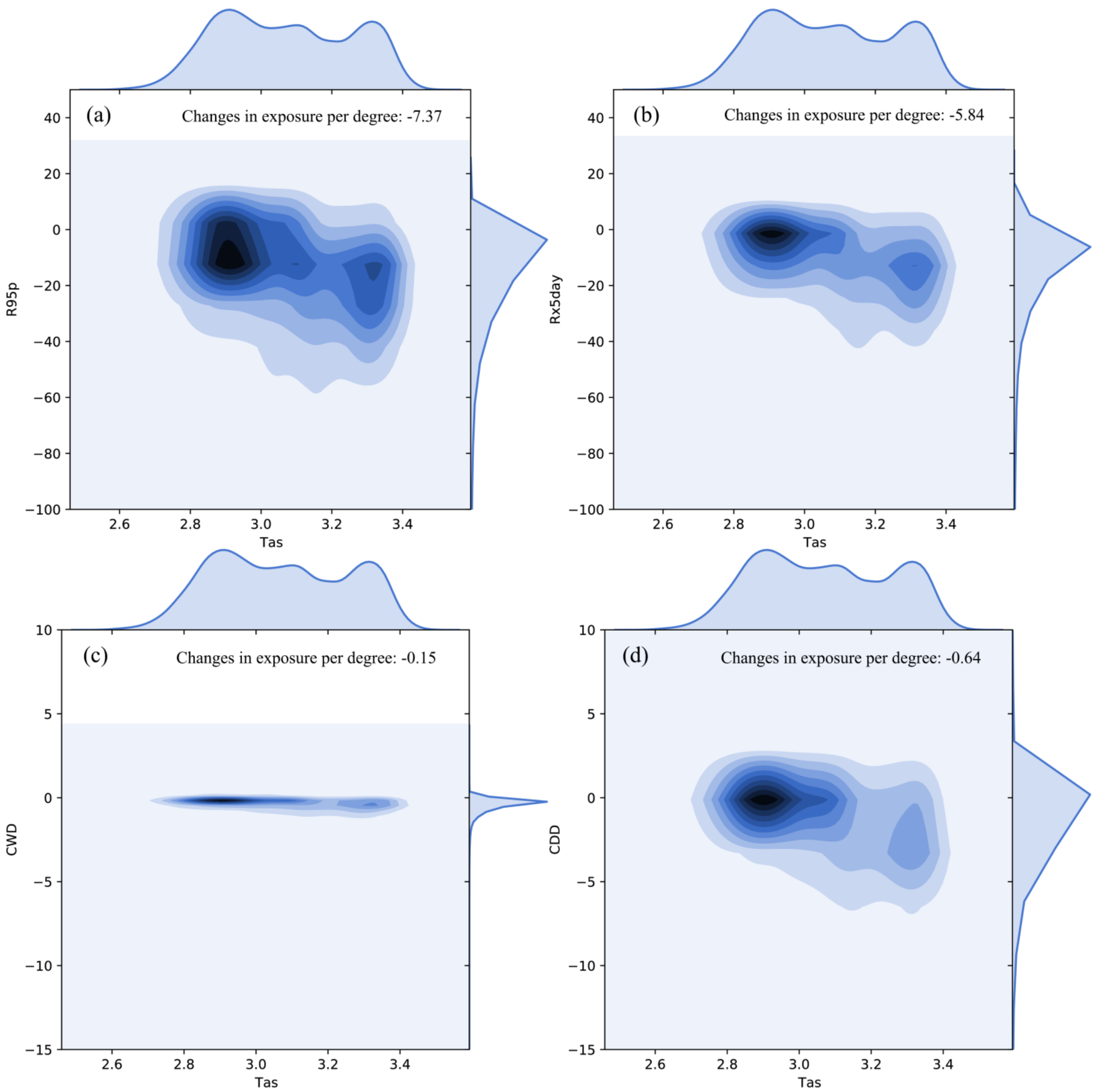

Figure 11. Kernel density plots of changes in population exposure to four precipitation extremes, R95p (unit: 10^4 person mm/°C), Rx5day (10^4 person mm/°C), CWDs (10^4 person day/°C) and CDDs (10^4 person days/°C), and air surface temperature over the JJJ region during the historical period (1991–1999) relative to the future period (2091–2099) with RCM_CLM_3km, as well as density curves. These changes are significant on the 0.05 level using a *t*-test with grid-point numbers of 12,925 (R95p), 25,251 (Rx5day), 32,178 (CWDs) and 27,451 (CDDs) among the total sample size of 36098.

In summary, the changes in total population exposure to the four precipitation extreme indices in this study were found to have generally decreased over most areas of the JJJ region. Changes in the future population and the extreme indices R95p and Rx5day will contribute moderately to changes in the total exposure over JJJ, while the population will dominantly impact the total exposure to CDDs. In addition, expected changes in total exposure to precipitation extremes per degree of warming were quantified over JJJ during 2091–2099 and compared with those of the historical period of 1991–1999.

4. Discussion

The regional climate model on the convection-permitting scale presented a good performance in simulating the regional climate, especially precipitation extremes, which usually show high spatiotemporal variations [66,98]. Benefitting from their high spatial resolutions on the kilometer scale, RCMs on the CP scale could capture more details of regional climate conditions [56] and better simulate land–atmospheric interactions, especially over areas with frequent anthropogenic activities, such as urban areas [68]. The present study has firstly analyzed changes in precipitation extremes with RegCM4 on the CP scale over the JJJ urban agglomeration with fast urbanization and rapid population growth.

The risks of precipitation extremes are impacted by the extremes themselves as well as the populations involved [31,76]. This study has investigated changes in precipitation extremes over the JJJ region as well as population exposure to extremes by RegCM4 with a non-hydrostatic dynamic core and a fine spatial resolution of 3 km and revealed the possible reason of these changes from annual or seasonal global atmospheric circulation. As in the previous study, the changes in precipitation extremes presented large spatial variations under climate change [48,68] due to too many physical processes being involved [99]. This study has focused on the impacts of current and future GCM forcing to precipitation extremes without land use changes. Since precipitation extremes are also affected by regional land–atmospheric interactions, such as evapotranspiration and land use; the contributions of global circulation and regional land–atmospheric interactions should be deeply investigated, and the performance of dynamic downscaling in simulating precipitation extremes could be evaluated in more detail, such as with regard to added values [100,101].

To better investigate the population's exposure to climate extremes, population policies should also be considered, as this might greatly affect population sizes and spatial distribution [95]. For example, the number of permanent residents in Beijing was restricted to 23 million in 2020 [102]. This study has compared the changes in the population exposure to precipitation extremes during the historical period from 1991 to 1999 and projected for the future period from 2091 to 2099, and different selections of historical and future periods might present different conclusions. In our future work, more recent historical populations will be adopted and precipitation extremes will also be simulated for the same time periods. These conclusions are model-dependent, and more simulations should be carried out to reduce uncertainties due to RCMs, GCMs and their different experimental setups. This could be carried out by using the multiple RCMs that participate in CORDEX [45,103] and with more GCM forcing in CMIP5 or CMIP6. Compound climate extremes usually result in greater impacts on human lives and society [104,105]. The population's exposure to compound extremes should also be investigated on the convection-permitting scale in future studies.

5. Conclusions

Warmer climates increase the ability of the atmosphere to hold more water vapor [1] and impact the occurrence of precipitation as well as precipitation extremes [106]. In the present study, changes in precipitation extremes and the population exposure to these extremes have been projected for the future period of 2091–2099 relative to those for the historical period of 1991–1999 in in China and the JJJ urban agglomeration, with spatial resolutions of 12 km and 3 km, respectively. The percentage contributions of the three components of total exposure, precipitation extremes multiplied by changes in the population amount, changes in precipitation extremes multiplied by the population amount and the multiplication of the changes in precipitation extremes by the changes in the population amount, were then investigated [107]. Additionally, changes in the population exposure to precipitation extremes for each degree of local warming were calculated for the JJJ region.

First, RegCM4 with a hydrostatic dynamic core at a spatial resolution of 12km was run over East Asia, with the whole of China included, for the historical and future periods, supported by high-resolution MPI-ESM1.2-HR in CMIP6 under the middle SSP245 scenario [80]. Results above 12 km were then used to derive the initial and boundary conditions to force RegCM4-NH at a spatial resolution of 3 km over the JJJ region. The performances of RegCM4 with hydrostatic and non-hydrostatic dynamic cores in China and over the JJJ region have been investigated that RegCM4-NH could simulate more detailed spatial distribution of precipitation over the JJJ region but with large spatial variations, as has been mentioned in other studies [68].

The heavy precipitation extremes R95p and Rx5day are projected to increase in the majority of China while decreasing over the JJJ region, which is consistent with previous studies [48,108]. These changes might be caused by slight increases in specific humidity over the JJJ region in the future, with moderate increases in the rest of China. On the other hand, land surface conditions such as land use and topography profoundly impact precipitation extremes through land–atmospheric interactions. RegCM4-NH, with a higher spatial resolution of 3 km, might better simulate such local interactions than can RCMs with hydrostatic dynamic cores [54]. On the other hand, more precise descriptions of physical processes and basis data, with higher resolutions consistent with RegCM4-NH, should be developed to improve RegCM4-NH simulation further.

Finally, changes in population exposure to precipitation extremes were investigated over the JJJ region. The population densities in China and JJJ are expected to decrease in general by 2100, except in some downtown areas of JJJ, where more people are expected to migrate from rural to urban areas with already high population densities. The population exposure to precipitation extremes is projected to decrease over most areas of the JJJ region. The contributions of changes in precipitation extremes and the population amount to the total exposure were then investigated [106]. The future population amount and precipitation extremes R95p and Rx5day were projected to equally contribute to changes in the total exposure over the JJJ region, while changes in the population amount were the dominant factor that would impact the total exposure to CDDs. Additionally, changes in population exposure to precipitation extremes under each degree of local warming were quantified.

The present study has had some limitations. One is that only one GCM was used to force the RCM RegCM4, and the conclusion was model-dependent [109]. Multiple RCMs forced by several GCMs might be better to reduce model uncertainties of precipitation simulation. Another limitation is that this study investigated changes in precipitation extremes due to the differences in current and future CMIP6 forcing without a land use change effect. In our following work, the contributions of changes in GCM forcing and land use changes during a more recent historical period with longer time span (such as 1985–2014) and a future period will be analyzed in more detail, as will the contributions of atmospheric circulation and local land–atmospheric interaction.

Author Contributions: P.Q.: formal analysis; investigation; visualization, project administration, funding acquisition; writing—original draft. Z.X.: funding acquisition, writing, reviewing and editing. B.J.: funding acquisition; writing, reviewing and editing. R.H.: writing, reviewing and editing. B.L.: writing, reviewing and editing. All authors have read and agreed to the published version of the manuscript.

Funding: This study was supported by the National Key Research and Development Program of China (Grant No. 2019YFA0606903), the National Natural Science Foundation of China (Grant No. 42075162), the Youth Innovation Promotion Association CAS (2021073) and the National Key Scientific and Technological Infrastructure project "Earth System Science Numerical Simulator Facility" (EarthLab).

Institutional Review Board Statement: Not applicable.

Informed Consent Statement: Not applicable.

Data Availability Statement: Spatiotemporal population data are available from https://www.cgd.ucar.edu/iam/modeling/spatial-population-scenarios.html (accessed on 1 July 2022). CMIP6 data can be downloaded from https://esgf-node.llnl.gov/search/cmip6/ (accessed on 1 July 2022).

Conflicts of Interest: The authors declare no conflict of interest.

References

1. O'Gorman, P.A. Precipitation Extremes Under Climate Change. *Curr. Clim. Chang. Rep.* **2015**, *1*, 49–59. [CrossRef]
2. Hegerl, G.C.; Black, E.; Allan, R.P.; Ingram, W.J.; Polson, D.; Trenberth, K.E.; Chadwick, R.S.; Arkin, P.A.; Sarojini, B.B.; Becker, A.; et al. Challenges in Quantifying Changes in the Global Water Cycle. *Bull. Am. Meteorol. Soc.* **2015**, *96*, 1097–1115. [CrossRef]
3. Tian, B.R.; Chen, H.; Yin, J.B.; Liao, Z.; Li, N.; He, S.K. Global scaling of precipitation extremes using near-surface air temperature and dew point temperature. *Environ. Res. Lett.* **2023**, *18*, 034016. [CrossRef]
4. Qin, P.H.; Xie, Z.H.; Zou, J.; Liu, S.; Chen, S. Future Precipitation Extremes in China under Climate Change and Their Physical Quantification Based on a Regional Climate Model and CMIP5 Model Simulations. *Adv. Atmos. Sci.* **2021**, *38*, 460–479. [CrossRef]
5. Patricola, C.M.; Wehner, M.F.; Bercos-Hickey, E.; Maciel, F.V.; May, C.; Mak, M.; Yip, O.; Roche, A.M.; Leal, S. Future changes in extreme precipitation over the San Francisco Bay Area: Dependence on atmospheric river and extratropical cyclone events. *Weather Clim. Extrem.* **2022**, *36*, 100440. [CrossRef]
6. Vergara-Temprado, J.; Ban, N.; Schar, C. Extreme Sub-Hourly Precipitation Intensities Scale Close to the Clausius-Clapeyron Rate Over Europe. *Geophys. Res. Lett.* **2021**, *48*, e2020GL089506. [CrossRef]
7. Lenderink, G.; Barbero, R.; Loriaux, J.M.; Fowler, H.J. Super-Clausius-Clapeyron Scaling of Extreme Hourly Convective Precipitation and Its Relation to Large-Scale Atmospheric Conditions. *J. Clim.* **2017**, *30*, 6037–6052. [CrossRef]
8. Guo, Q.; Hibino, K. Physical responses of Baiu extreme precipitation to future warming: Examples of the 2018 and 2020 western Japan events. *Weather Clim. Extrem.* **2023**, *39*, 100547. [CrossRef]
9. John, A.; Douville, H.; Ribes, A.; Yiou, P. Quantifying CMIP6 model uncertainties in extreme precipitation projections. *Weather Clim. Extrem.* **2022**, *36*, 100435. [CrossRef]
10. IPCC. *Climate Change 2021: The Physical Science Basis. Contribution of Working Group I to the Sixth Assessment Report of the Intergovernmental Panel on Climate Change*; Cambridge University Press: Cambridge, UK, 2021.
11. Delgado-Torres, C.; Donat, M.G.; Soret, A.; Gonzalez-Reviriego, N.; Bretonniere, P.A.; Ho, A.C.; Perez-Zanon, N.; Cabre, M.S.; Doblas-Reyes, F.J. Multi-annual predictions of the frequency and intensity of daily temperature and precipitation extremes. *Environ. Res. Lett.* **2023**, *18*, 034031. [CrossRef]
12. Kumari, A.; Kumar, P. Evaluation and future projection of the extreme precipitation over India and its homogeneous regions: A regional earth system model perspective. *Int. J. Climatol.* **2023**, *43*, 3679–3697. [CrossRef]
13. Yang, L.C.; Franzke, C.L.E.; Duan, W.S. Evaluation and projections of extreme precipitation using a spatial extremes framework. *Int. J. Climatol.* **2023**, *43*, 3453–3475. [CrossRef]
14. Xu, L.L.; Zhang, T.T.; Yu, W.; Yang, S. Changes in concurrent precipitation and temperature extremes over the Asian monsoon region: Observation and projection. *Environ. Res. Lett.* **2023**, *18*, 044021. [CrossRef]
15. Eyring, V.; Bony, S.; Meehl, G.A.; Senior, C.A.; Stevens, B.; Stouffer, R.J.; Taylor, K.E. Overview of the Coupled Model Intercomparison Project Phase 6 (CMIP6) experimental design and organization. *Geosci. Model Dev.* **2016**, *9*, 1937–1958. [CrossRef]
16. Taylor, K.E.; Stouffer, R.J.; Meehl, G.A. An Overview of Cmip5 and the Experiment Design. *Bull. Am. Meteorol. Soc.* **2012**, *93*, 485–498. [CrossRef]
17. Kim, Y.H.; Min, S.K.; Zhang, X.B.; Sillmann, J.; Sandstad, M. Evaluation of the CMIP6 multi-model ensemble for climate extreme indices. *Weather Clim. Extrem.* **2020**, *29*, 100269. [CrossRef]
18. Babaousmail, H.; Hou, R.T.; Ayugi, B.; Sian, K.T.C.L.K.; Ojara, M.; Mumo, R.; Chehbouni, A.; Ongoma, V. Future changes in mean and extreme precipitation over the Mediterranean and Sahara regions using bias-corrected CMIP6 models. *Int. J. Climatol.* **2022**, *42*, 7280–7297. [CrossRef]
19. Sian, K.T.C.L.K.; Hagan, D.F.T.; Ayugi, B.O.; Nooni, I.K.; Ullah, W.; Babaousmail, H.; Ongoma, V. Projections of precipitation extremes based on bias-corrected Coupled Model Intercomparison Project phase 6 models ensemble over southern Africa. *Int. J. Climatol.* **2022**, *42*, 8269–8289. [CrossRef]
20. Sojan, J.M.; Srivastav, R.; Meghana, N. Regional non-stationary future extreme rainfall under changing climate over Asian Monsoon Region. *Atmos. Res.* **2023**, *284*, 106592. [CrossRef]
21. Dong, T.Y.; Dong, W.J. Evaluation of extreme precipitation over Asia in CMIP6 models. *Clim. Dyn.* **2021**, *57*, 1751–1769. [CrossRef]
22. Ge, F.; Zhu, S.P.; Luo, H.L.; Zhi, X.F.; Wang, H. Future changes in precipitation extremes over Southeast Asia: Insights from CMIP6 multi-model ensemble. *Environ. Res. Lett.* **2021**, *16*, 024013. [CrossRef]
23. Zhu, H.H.; Jiang, Z.H.; Li, L. Projection of climate extremes in China, an incremental exercise from CMIP5 to CMIP6. *Sci. Bull.* **2021**, *66*, 2528–2537. [CrossRef] [PubMed]
24. Moradian, S.; Haghighi, A.T.; Asadi, M.; Mirbagheri, S.A. Future Changes in Precipitation Over Northern Europe Based on a Multi-model Ensemble from CMIP6: Focus on Tana River Basin. *Water Resour. Manag.* **2023**, *37*, 2447–2463. [CrossRef]
25. Srivastava, A.; Grotjahn, R.; Ullrich, P.A. Evaluation of historical CMIP6 model simulations of extreme precipitation over contiguous US regions. *Weather Clim. Extrem.* **2020**, *29*, 100268. [CrossRef]

26. Olmo, M.E.; Balmaceda-Huarte, R.; Bettolli, M.L. Multi-model ensemble of statistically downscaled GCMs over southeastern South America: Historical evaluation and future projections of daily precipitation with focus on extremes. *Clim. Dyn.* **2022**, *59*, 3051–3068.
27. De Medeiros, F.J.; de Oliveira, C.P.; Avila-Diaz, A. Evaluation of extreme precipitation climate indices and their projected changes for Brazil: From CMIP3 to CMIP6. *Weather Clim. Extrem.* **2022**, *38*, 100511. [CrossRef]
28. Jong, B.T.; Delworth, T.L.; Cooke, W.F.; Tseng, K.C.; Murakami, H. Increases in extreme precipitation over the Northeast United States using high-resolution climate model simulations. *Npj Clim. Atmos. Sci.* **2023**, *6*, 18. [CrossRef]
29. Pfahl, S.; O'Gorman, P.A.; Fischer, E.M. Understanding the regional pattern of projected future changes in extreme precipitation. *Nat. Clim. Chang.* **2017**, *7*, 423–427. [CrossRef]
30. Xie, S.P.; Deser, C.; Vecchi, G.A.; Collins, M.; Delworth, T.L.; Hall, A.; Hawkins, E.; Johnson, N.C.; Cassou, C.; Giannini, A.; et al. Towards predictive understanding of regional climate change. *Nat. Clim. Chang.* **2015**, *5*, 921–930. [CrossRef]
31. Qin, P.H. More than six billion people encountering more exposure to extremes with 1.5 degrees C and 2.0 degrees C warming. *Atmos. Res.* **2022**, *273*, 106165. [CrossRef]
32. Bador, M.; Boe, J.; Terray, L.; Alexander, L.V.; Baker, A.; Bellucci, A.; Haarsma, R.; Koenigk, T.; Moine, M.P.; Lohmann, K.; et al. Impact of Higher Spatial Atmospheric Resolution on Precipitation Extremes Over Land in Global Climate Models. *J. Geophys. Res. Atmos.* **2020**, *125*, e2019JD032184. [CrossRef]
33. Davolio, S.; Vercellino, M.; Miglietta, M.M.; Pitura, L.D.; Laviola, S.; Levizzani, V. The influence of an atmospheric river on a heavy precipitation event over the western Alps. *Weather Clim. Extrem.* **2023**, *39*, 100542. [CrossRef]
34. Huang, X.Y.; Swain, D.L.; Hall, A.D. Future precipitation increase from very high resolution ensemble downscaling of extreme atmospheric river storms in California. *Sci. Adv.* **2020**, *6*, eaba1323. [CrossRef] [PubMed]
35. Whan, K.; Sillmann, J.; Schaller, N.; Haarsma, R. Future changes in atmospheric rivers and extreme precipitation in Norway. *Clim. Dyn.* **2020**, *54*, 2071–2084. [CrossRef]
36. Zhao, M. Simulations of Atmospheric Rivers, Their Variability, and Response to Global Warming Using GFDL's New High-Resolution General Circulation Model. *J. Clim.* **2020**, *33*, 10287–10303. [CrossRef]
37. Gori, A.; Lin, N.; Xi, D.Z.; Emanuel, K. Tropical cyclone climatology change greatly exacerbates US extreme rainfall-surge hazard. *Nat. Clim. Chang.* **2022**, *12*, 491. [CrossRef]
38. Gao, T.; Zou, L.W.; Cao, F.Q.; Zhan, J.J. Impacts of tropical cyclones on summertime short-duration precipitation extremes over the middle-lower reaches of the Yangtze River valley. *Atmos. Res.* **2023**, *282*, 106520. [CrossRef]
39. Zhang, S.Y.; Wang, M.H.; Wang, L.N.; Liang, X.Z.; Sun, C.; Li, Q.Q. Sensitivity of the simulation of extreme precipitation events in China to different cumulus parameterization schemes and the underlying mechanisms. *Atmos. Res.* **2023**, *285*, 106636. [CrossRef]
40. Ehmele, F.; Kautz, L.A.; Feldmann, H.; Pinto, J.G. Long-term variance of heavy precipitation across central Europe using a large ensemble of regional climate model simulations. *Earth Syst. Dyn.* **2020**, *11*, 469–490. [CrossRef]
41. Da Silva, M.L.; de Oliveira, C.P.; Silva, C.M.; de Araujo, J.M. Analysis of climate extremes indices in tropical South America through the RegCM4.7. *Int. J. Climatol.* **2023**, 1–26. [CrossRef]
42. Fan, Y.W.; Im, E.; Lan, C.W.; Lo, M.H. An increase in precipitation driven by irrigation over the North China Plain based on RegCM and WRF simulations. *J. Hydrometeorol.* **2023**, *24*, 1155–1173. [CrossRef]
43. Rendfrey, T.S.; Bukovsky, M.S.; McCrary, R.R.; Fuentes-Franco, R. An assessment of tropical cyclones in North American CORDEX WRF simulations. *Weather Clim. Extrem.* **2021**, *34*, 100382. [CrossRef]
44. Qiu, Y.; Feng, J.M.; Yan, Z.W.; Wang, J.; Li, Z. High-resolution dynamical downscaling for regional climate projection in Central Asia based on bias-corrected multiple GCMs. *Clim. Dyn.* **2022**, *58*, 777–791. [CrossRef]
45. Diez-Sierra, J.; Iturbide, M.; Gutierrez, J.M.; Fernandez, J.; Milovac, J.; Cofino, A.S.; Cimadevilla, E.; Nikulin, G.; Levavasseur, G.; Kjellstrom, E.; et al. The Worldwide C3S CORDEX Grand Ensemble: A Major Contribution to Assess Regional Climate Change in the IPCC AR6 Atlas. *Bull. Am. Meteorol. Soc.* **2022**, *103*, E2804–E2826. [CrossRef]
46. Giorgi, F.; Coppola, E.; Solmon, F.; Mariotti, L.; Sylla, M.B.; Bi, X.; Elguindi, N.; Diro, G.T.; Nair, V.; Giuliani, G.; et al. RegCM4: Model description and preliminary tests over multiple CORDEX domains. *Clim. Res.* **2012**, *52*, 7–29. [CrossRef]
47. Da Silva, M.L.; de Oliveira, C.P.; Silva, C.M.S.E.; de Araujo, J.M. Dynamic downscaling of climate simulations and projected changes in tropical South America using RegCM4.7. *Int. J. Climatol.* **2023**, *43*, 3391–3415. [CrossRef]
48. Zou, L.W.; Zhou, T.J. Mean and extreme precipitation changes over China under SSP scenarios: Results from high-resolution dynamical downscaling for CORDEX East Asia. *Clim. Dyn.* **2022**, *58*, 1015–1031. [CrossRef]
49. Luo, J.X.; Lyu, S.H.; Fang, X.W.; Liu, Y.G. Trends in the frozen ground temperature on the Tibetan Plateau simulated by RegCM4.7-CLM4.5. *Theor. Appl. Climatol.* **2021**, *145*, 891–901. [CrossRef]
50. Anwar, S.A.; Reboita, M.S.; Llopart, M. On the sensitivity of the Amazon surface climate to two land-surface hydrology schemes using a high-resolution regional climate model (RegCM4). *Int. J. Climatol.* **2022**, *42*, 2311–2327. [CrossRef]
51. Wu, J.; Gao, X.J.; Zhu, Y.M.; Shi, Y.; Giorgi, F. Projection of the Future Changes in Tropical Cyclone Activity Affecting East Asia over the Western North Pacific Based on Multi-RegCM4 Simulations. *Adv. Atmos. Sci.* **2021**, *39*, 284–303. [CrossRef]
52. Shahi, N.K.; Das, S.; Ghosh, S.; Maharana, P.; Rai, S. Projected changes in the mean and intra-seasonal variability of the Indian summer monsoon in the RegCM CORDEX-CORE simulations under higher warming conditions. *Clim. Dyn.* **2021**, *57*, 1489–1506. [CrossRef]

53. Gao, S.B. Dynamical downscaling of surface air temperature and precipitation using RegCM4 and WRF over China. *Clim. Dyn.* **2020**, *55*, 1283–1302. [CrossRef]
54. Coppola, E.; Paolo Stocchi, E.P.; Alavez, J.A.T.; Glazer, R.; Giuliani, G.; Sante, F.D.; Nogherotto, R.; Giorgi, F. Non-Hydrostatic RegCM4 (RegCM4-NH): Model description and case studies over multiple domains. *Geosci. Model Dev.* **2021**, *14*, 7705–7723. [CrossRef]
55. Coppola, E.; Sobolowski, S.; Pichelli, E.; Raffaele, F.; Ahrens, B.; Anders, I.; Ban, N.; Bastin, S.; Belda, M.; Belusic, D.; et al. A first-of-its-kind multi-model convection permitting ensemble for investigating convective phenomena over Europe and the Mediterranean. *Clim. Dyn.* **2020**, *55*, 3–34. [CrossRef]
56. Gutowski, W.J.; Ullrich, P.A.; Hall, A.; Leung, L.R.; O'Brien, T.A.; Patricola, C.M.; Arritt, R.W.; Bukovsky, M.S.; Calvin, K.V.; Feng, Z.; et al. The Ongoing Need for High-Resolution Regional Climate Models: Process Understanding and Stakeholder Information. *Bull. Am. Meteorol. Soc.* **2020**, *101*, E664–E683. [CrossRef]
57. Prein, A.F.; Langhans, W.; Fosser, G.; Ferrone, A.; Ban, N.; Goergen, K.; Keller, M.; Tolle, M.; Gutjahr, O.; Feser, F.; et al. A review on regional convection-permitting climate modeling: Demonstrations, prospects, and challenges. *Rev. Geophys.* **2015**, *53*, 323–361. [CrossRef] [PubMed]
58. Takayabu, I.; Rasmussen, R.; Nakakita, E.; Prein, A.; Kawase, H.; Watanabe, S.I.; Adachi, S.A.; Takemi, T.; Yamaguchi, K.; Osakada, Y.; et al. Convection-Permitting Models for Climate Research. *Bull. Am. Meteorol. Soc.* **2022**, *103*, E77–E82. [CrossRef]
59. Ban, N.; Caillaud, C.; Coppola, E.; Pichelli, E.; Sobolowski, S.; Adinolfi, M.; Ahrens, B.; Alias, A.; Anders, I.; Bastin, S.; et al. The first multi-model ensemble of regional climate simulations at kilometer-scale resolution, part I: Evaluation of precipitation. *Clim. Dyn.* **2021**, *57*, 275–302. [CrossRef]
60. Perez, J.C.; Exposito, F.J.; Gonzalez, A.; Diaz, J.P. Climate projections at a convection-permitting scale of extreme temperature indices for an archipelago with a complex microclimate structure. *Weather Clim. Extrem.* **2022**, *36*, 100459. [CrossRef]
61. Lucas-Picher, P.; Brisson, E.; Caillaud, C.; Alias, A.; Nabat, P.; Lemonsu, A.; Poncet, N.; Hernandez, V.E.C.; Michau, Y.; Doury, A.; et al. Evaluation of the convection-permitting regional climate model CNRM-AROME41t1 over Northwestern Europe. *Clim. Dyn.* **2023**. [CrossRef]
62. Yun, Y.X.; Liu, C.H.; Luo, Y.L.; Gao, W.H. Warm-season mesoscale convective systems over eastern China: Convection-permitting climate model simulation and observation. *Clim. Dyn.* **2021**, *57*, 3599–3617. [CrossRef]
63. Poujol, B.; Mooney, P.A.; Sobolowski, S.P. Physical processes driving intensification of future precipitation in the mid- to high latitudes. *Environ. Res. Lett.* **2021**, *16*, 034051. [CrossRef]
64. Feijoo, M.; Solman, S. Convection-permitting modeling strategies for simulating extreme rainfall events over Southeastern South America. *Clim. Dyn.* **2022**, *59*, 2549–2569. [CrossRef]
65. Luu, L.N.; Vautard, R.; Yiou, P.; Soubeyroux, J.M. Evaluation of convection-permitting extreme precipitation simulations for the south of France. *Earth Syst. Dyn.* **2022**, *13*, 687–702. [CrossRef]
66. Lucas-Picher, P.; Argueso, D.; Brisson, E.; Tramblay, Y.; Berg, P.; Lemonsu, A.; Kotlarski, S.; Caillaud, C. Convection-permitting modeling with regional climate models: Latest developments and next steps. *Wires Clim. Chang.* **2021**, *12*, e731. [CrossRef]
67. Gao, Y.H.; Xu, J.W.; Zhang, M.; Liu, Z.Y.; Dan, J.Y. Regional climate dynamical downscaling over the Tibetan Plateau-From quarter-degree to kilometer-scale. *Sci. China Earth Sci.* **2022**, *65*, 2237–2247. [CrossRef]
68. Nguyen-Xuan, T.; Lam, S.L.; Giorgi, F.; Coppola, E.; Giuliani, G.; Gao, X.J.; Im, E.S. Evaluation of the performance of the non-hydrostatic RegCM4 (RegCM4-NH) over Southeastern China. *Clim. Dyn.* **2022**, *58*, 1419–1437. [CrossRef]
69. Pichelli, E.; Coppola, E.; Sobolowski, S.; Ban, N.; Giorgi, F.; Stocchi, P.; Alias, A.; Belusic, D.; Berthou, S.; Caillaud, C.; et al. The first multi-model ensemble of regional climate simulations at kilometer-scale resolution part 2: Historical and future simulations of precipitation. *Clim. Dyn.* **2021**, *56*, 3581–3602. [CrossRef]
70. Si, P.; Wang, M.; Li, M.C.; Wang, Y.A.; Guo, Y.D.; Yang, Y.J.; Wang, J. The observed features and some possible reasons of annual temperature extremes over Beijing–Tianjin–Hebei region for a century long-term based on newly constructed daily observations. *Int. J. Climatol.* **2023**, *43*, 4248–4268. [CrossRef]
71. Zheng, Z.Y.; Dong, W.J.; Yan, D.D.; Guo, Y.; Wei, Z.G.; Chou, J.M.; Zhu, X.; Wen, X.H. Relative contributions of urbanization and greenhouse gases concentration on future climate over Beijing-Tianjin-Hebei region in China. *Clim. Dyn.* **2022**, *58*, 1085–1105. [CrossRef]
72. Yuan, Y.F.; Zhai, P.M.; Chen, Y.; Li, J. Hourly extreme precipitation changes under the influences of regional and urbanization effects in Beijing. *Int. J. Climatol.* **2021**, *41*, 1179–1189. [CrossRef]
73. Jones, B.; Tebaldi, C.; O'Neill, B.C.; Oleson, K.; Gao, J. Avoiding population exposure to heat-related extremes: Demographic change vs climate change. *Clim. Chang.* **2018**, *146*, 423–437. [CrossRef]
74. Thiery, W.; Lange, S.; Rogelj, J.; Schleussner, C.F.; Gudmundsson, L.; Seneviratne, S.I.; Andrijevic, M.; Frieler, K.; Emanuel, K.; Geiger, T.; et al. Intergenerational inequities in exposure to climate extremes Young generations are severely threatened by climate change. *Science* **2021**, *374*, 158–160. [CrossRef]
75. Wang, A.Q.; Tao, H.; Ding, G.; Zhang, B.L.; Huang, J.L.; Wu, Q.Y. Global cropland exposure to extreme compound drought heatwave events under future climate change. *Weather Clim. Extrem.* **2023**, *40*, 100559. [CrossRef]
76. Shen, L.C.; Wen, J.H.; Zhang, Y.Q.; Ullah, S.; Cheng, J.Y.; Meng, X.C. Changes in population exposure to extreme precipitation in the Yangtze River Delta, China. *Clim. Serv.* **2022**, *27*, 100317. [CrossRef]

77. Ullah, S.; You, Q.L.; Chen, D.L.; Sachindra, D.A.; AghaKouchak, A.; Kang, S.C.; Li, M.C.; Zhai, P.M.; Ullah, W. Future Population Exposure to Daytime and Nighttime Heat Waves in South Asia. *Earths Future* **2022**, *10*, e2021EF002511. [CrossRef]
78. Tuholske, C.; Caylor, K.; Funk, C.; Verdin, A.; Sweeney, S.; Grace, K.; Peterson, P.; Evans, T. Global urban population exposure to extreme heat. *Proc. Natl. Acad. Sci. USA* **2021**, *118*, e2024792118. [CrossRef]
79. Wu, X.Y.; Hao, Z.C.; Tang, Q.H.; Zhang, X.; Feng, S.F.; Hao, F.H. Population exposure to compound dry and hot events in China under 1.5 and 2 degrees C global warming. *Int. J. Climatol.* **2021**, *41*, 5766–5775. [CrossRef]
80. Fricko, O.; Havlik, P.; Rogelj, J.; Klimont, Z.; Gusti, M.; Johnson, N.; Kolp, P.; Strubegger, M.; Valin, H.; Amann, M.; et al. The marker quantification of the Shared Socioeconomic Pathway 2: A middle-of-the-road scenario for the 21st century. *Glob. Environ. Chang.* **2017**, *42*, 251–267. [CrossRef]
81. Muller, W.A.; Jungclaus, J.H.; Mauritsen, T.; Baehr, J.; Bittner, M.; Budich, R.; Bunzel, F.; Esch, M.; Ghosh, R.; Haak, H.; et al. A Higher-resolution Version of the Max Planck Institute Earth System Model (MPI-ESM1.2-HR). *J. Adv. Model. Earth Syst.* **2018**, *10*, 1383–1413. [CrossRef]
82. Oleson, K.W.; Lawrence, D.M.; Bonan, G.B.; Drewniak, B.; Huang, M.; Koven, C.D.; Levis, S.; Li, F.; Riley, W.J.; Subin, Z.M.; et al. *Technical Description of version 4.5 of the Community Land Model (CLM)*; NCAR/TN-503+STR; NCAR: Boulder, CO, USA, 2013.
83. Gao, J. *Downscaling Global Spatial Population Projections from 1/8-Degree to 1-Km Grid Cells*; NCAR Technical Note NCAR/TN-537+STR; National Center for Atmospheric Research: Boulder, CO, USA, 2017.
84. Jones, B.; O'Neill, B.C. Spatially explicit global population scenarios consistent with the Shared Socioeconomic Pathways. *Environ. Res. Lett.* **2016**, *11*, 084003. [CrossRef]
85. Li, S.H.; Otto, F.E.L.; Harrington, L.J.; Sparrow, S.N.; Wallom, D.C.H. A pan-South-America assessment of avoided exposure to dangerous extreme precipitation by limiting to 1.5 degrees C warming. *Environ. Res. Lett.* **2020**, *15*, 054005. [CrossRef]
86. Grell, G.A. Prognostic Evaluation of Assumptions Used by Cumulus Parameterizations. *Mon. Wea. Rev.* **1993**, *121*, 764–787. [CrossRef]
87. Skamarock, W.C.; Klemp, J.B.; Dudhia, J.; Gill, D.O.; Barker, D.M.; Duda, M.G.; Huang, X.Y.; Wang, W.; Powers, J.G. *A Description of the Advanced Research WRF Version 3*; NCAR/TN-475+STR; National Center for Atmospheric Research: Boulder, CO, USA, 2008.
88. Pendergrass, A.G. What precipitation is extreme? *Science* **2018**, *360*, 1072–1073. [CrossRef] [PubMed]
89. Zhang, X.B.; Alexander, L.; Hegerl, G.C.; Jones, P.; Tank, A.K.; Peterson, T.C.; Trewin, B.; Zwiers, F.W. Indices for monitoring changes in extremes based on daily temperature and precipitation data. *Wires Clim. Chang.* **2011**, *2*, 851–870. [CrossRef]
90. Imran, H.M.; Kala, J.; Uddin, S.; Islam, A.K.M.S.; Acharya, N. Spatiotemporal analysis of temperature and precipitation extremes over Bangladesh using a novel gridded observational dataset. *Weather Clim. Extrem.* **2023**, *39*, 100544. [CrossRef]
91. Lagos-Zuniga, M.; Balmaceda-Huarte, R.; Regoto, P.; Torrez, L.; Olmo, M.; Lyra, A.; Pareja-Quispe, D.; Bettolli, M.L. Extreme indices of temperature and precipitation in South America: Trends and intercomparison of regional climate models. *Clim. Dyn.* **2022**. [CrossRef]
92. Wei, W.; Zou, S.; Duan, W.L.; Chen, Y.N.; Li, S.; Zhou, Y.Q. Spatiotemporal variability in extreme precipitation and associated large-scale climate mechanisms in Central Asia from 1950 to 2019. *J. Hydrol.* **2023**, *620*, 129417. [CrossRef]
93. Feng, T.C.; Zhu, X.; Dong, W.J. Historical assessment and future projection of extreme precipitation in CMIP6 models: Global and continental. *Int. J. Climatol.* **2023**, *43*, 4119–4135. [CrossRef]
94. Seneviratne, S.I.; Hauser, M. Regional Climate Sensitivity of Climate Extremes in CMIP6 Versus CMIP5 Multimodel Ensembles. *Earths Future* **2020**, *8*, e2019EF001474. [CrossRef]
95. Chen, Y.D.; Guo, F.; Wang, J.C.; Cai, W.J.; Wang, C.; Wang, K.C. Provincial and gridded population projection for China under shared socioeconomic pathways from 2010 to 2100. *Sci. Data* **2020**, *7*, 83. [CrossRef] [PubMed]
96. Wang, K.C.; Jiang, S.J.; Wang, J.K.; Zhou, C.L.; Wang, X.Y.; Lee, X. Comparing the diurnal and seasonal variabilities of atmospheric and surface urban heat islands based on the Beijing urban meteorological network. *J. Geophys. Res. Atmos.* **2017**, *122*, 2131–2154. [CrossRef]
97. Jones, B.; O'Neill, B.C.; McDaniel, L.; McGinnis, S.; Mearns, L.O.; Tebaldi, C. Future population exposure to US heat extremes. *Nat. Clim. Chang.* **2015**, *5*, 652–655. [CrossRef]
98. Fosser, G.; Kendon, E.J.; Stephenson, D.; Tucker, S. Convection-Permitting Models Offer Promise of More Certain Extreme Rainfall Projections. *Geophys. Res. Lett.* **2020**, *47*, e2020GL088151. [CrossRef]
99. Tang, Y.; Huang, A.N.; Wu, P.L.; Huang, D.Q.; Xue, D.K.; Wu, Y. Drivers of Summer Extreme Precipitation Events Over East China. *Geophys. Res. Lett.* **2021**, *48*, e2021GL093670. [CrossRef]
100. Tamoffo, A.T.; Dosio, A.; Vondou, D.A.; Sonkoue, D. Process-Based Analysis of the Added Value of Dynamical Downscaling Over Central Africa. *Geophys. Res. Lett.* **2020**, *47*, e2020GL089702. [CrossRef]
101. Boker, B.; Laux, P.; Olschewski, P.; Kunstmann, H. Added value of an atmospheric circulation pattern-based statistical downscaling approach for daily precipitation distributions in complex terrain. *Int. J. Climatol.* **2023**, 1–24. [CrossRef]
102. Beijing Municipal Commission of Planning and Natural Resources. *Beijing City Master Plan (2016–2035)*; Beijing Municipal Commission of Planning and Natural Resources: Beijing, China, 2017. Available online: http://ghzrzyw.beijing.gov.cn/zhengwuxinxi/zxzt/bjcsztgh20162035/index.html (accessed on 1 July 2022). (In Chinese)
103. Gutowski, W.J.; Giorgi, F.; Timbal, B.; Frigon, A.; Jacob, D.; Kang, H.S.; Raghavan, K.; Lee, B.; Lennard, C.; Nikulin, G.; et al. WCRP COordinated Regional Downscaling EXperiment (CORDEX): A diagnostic MIP for CMIP6. *Geosci. Model Dev.* **2016**, *9*, 4087–4095. [CrossRef]

104. Sun, P.; Zou, Y.F.; Yao, R.; Ma, Z.C.; Bian, Y.J.; Ge, C.H.; Lv, Y.F. Compound and successive events of extreme precipitation and extreme runoff under heatwaves based on CMIP6 models. *Sci. Total Environ.* **2023**, *878*, 162980. [CrossRef]
105. Meng, Y.; Hao, Z.C.; Zhang, Y.; Zhang, X.; Hao, F.H. Projection of compound wind and precipitation extremes in China based on Phase 6 of the Coupled Model Intercomparison Project models. *Int. J. Climatol.* **2023**, *43*, 1396–1406. [CrossRef]
106. Chen, H.P.; Sun, J.Q. Significant Increase of the Global Population Exposure to Increased Precipitation Extremes in the Future. *Earths Future* **2021**, *9*, e2020EF001941. [CrossRef]
107. Chen, H.P.; Sun, J.Q. Increased population exposure to extreme droughts in China due to 0.5 degrees C of additional warming. *Environ. Res. Lett.* **2019**, *14*, 064011. [CrossRef]
108. Wu, X.J.; Wang, L.C.; Niu, Z.G.; Jiang, W.X.; Cao, Q. More extreme precipitation over the Yangtze River Basin, China: Insights from historical and projected perspectives. *Atmos. Res.* **2023**, *292*, 106883. [CrossRef]
109. Seo, G.Y.; Ahn, J.B.; Cha, D.H.; Suh, M.S.; Min, S.K.; Chang, E.C.; Byun, Y.H.; Kim, J.U. Evaluation of multi-RCM ensembles for simulating spatiotemporal variability of Asian summer monsoon precipitation in the CORDEX-East Asia Phase 2 domain. *Int. J. Climatol.* **2023**, *43*, 3710–3729. [CrossRef]